

Solution-Processed Perovskite Quantum Dot Quasi-BIC Laser from Miniaturized Low-Lateral-Loss Cavity

Di Xing, Mu-Hsin Chen, Zhiyu Wang, Chih-Zong Deng, Ya-Lun Ho, Bo-Wei Lin, Cheng-Chieh Lin, Chun-Wei Chen, and Jean-Jacques Delaunay*

Laser devices produced via solution-processed perovskite quantum dots (QDs) offer broad spectral tunability as well as ease of fabrication. Utilizing quasi-bound states in the continuum (quasi-BIC) modes, solution-processed QD laser devices have been demonstrated with a nanostructure coated in a thin-film gain media configuration. However, light leakage through thin-film guiding from the cavity side edges becomes more pronounced when shrinking the cavity size, posing challenges for the miniaturization of quasi-BIC-based lasers. Here, the fabrication of well-defined patterns of QDs via a solution process allows them to take advantage of the pattern edges to reduce losses through the cavity edges. A single-mode BIC laser is reported by using CsPbBr₃ QDs with a narrow linewidth of ≈ 0.1 nm. Importantly, a miniaturized quasi-BIC laser is realized with a device size as small as $10 \times 10 \mu\text{m}^2$, making it the smallest among existing solution-processed BIC lasers. This work provides a strategy for developing ultra-compact BIC lasers via solution-processed gain media.

1. Introduction

Solution-processed laser devices utilizing gain medium films obtained from dye-doped resists,^[1–3] perovskites,^[4–8] colloidal quantum wells,^[9–11] and colloidal quantum dots (QDs)^[12–18] have achieved significant progress. The ease of integration with other photonic components, low cost, and the potential for large-area fabrication technologies make them highly appealing for numerous applications, including integrated photonic circuitry,^[19,20] displays,^[21–23] communications,^[24] sensing, and biomedical fields.^[25,26] In the realm of solution-processed colloidal QDs, CsPbX₃ QDs have attracted great interest due to their remarkable optoelectronic properties, such as a high photoluminescence quantum yield (PLQY), narrow emission line widths, and the wide spectrum of tunable emission wavelengths.^[27–31] Unlike

other colloidal QDs, CsPbX₃ QDs can be easily synthesized on a large scale at a relatively low temperature. Furthermore, their high modal gain enables the realization of multiphoton pump lasers^[32] and achieves ultralow thresholds for amplified spontaneous emission (ASE) and lasing.^[30,33–35] These characteristics make them hold great promise for advancements in the field of solution-processed nanolasers.

In the field of nanophotonics, there has been a long-standing pursuit of achieving ultra-compact single-mode lasers. Besides an efficient gain medium, strong light confinement in the cavity is the most important step toward achieving miniaturized lasers. Optical bound states in the continuum (BIC) have demonstrated their versatility as a powerful tool for achieving light confinement and a substantial enhancement of the quality factor (Q factor) in periodic structures.^[36] BIC states provide a complete localized mode even though these states fall in the continuum of states above the light line, thus ensuring the complete suppression of radiative losses.^[36–38] In reality, an actual periodic structure supporting the BIC mode has a limited Q factor due to fabrication imperfections, material absorption, and the structure's finite size and is referred to as a quasi-BIC.^[36,39,40] Particularly, shrinking the size of the periodic structure will cause a dramatic drop in the Q factor due to the loss of light confinement from the quasi-BIC in the lateral direction.^[39,41] To achieve miniaturized BIC lasers, overcoming the large lateral losses in the finite-size cavities is highly desired.^[41,42] For now, some miniaturized

D. Xing, M.-H. Chen, Z. Wang, B.-W. Lin, J.-J. Delaunay
School of Engineering
The University of Tokyo
7-3-1 Hongo, Bunkyo-ku, Tokyo 113–8656, Japan
E-mail: jean@mech.t.u-tokyo.ac.jp

C.-Z. Deng
Advanced Research Laboratory, Technology Infrastructure Center, Technology Platform
Sony Group Corporation
4-14-1 Asahi-cho, Atsugi-shi 243-0014, Japan

Y.-L. Ho
Research Center for Electronic and Optical Materials
National Institute for Materials Science (NIMS)
1-1 Namiki, Tsukuba, Ibaraki 305-0044, Japan

C.-C. Lin, C.-W. Chen
Department of Materials Science and Engineering
National Taiwan University
No. 1, Sec. 4, Roosevelt Rd., Taipei 10617, Taiwan

The ORCID identification number(s) for the author(s) of this article can be found under <https://doi.org/10.1002/adfm.202314953>

© 2024 The Authors. Advanced Functional Materials published by Wiley-VCH GmbH. This is an open access article under the terms of the Creative Commons Attribution-NonCommercial-NoDerivs License, which permits use and distribution in any medium, provided the original work is properly cited, the use is non-commercial and no modifications or adaptations are made.

DOI: 10.1002/adfm.202314953

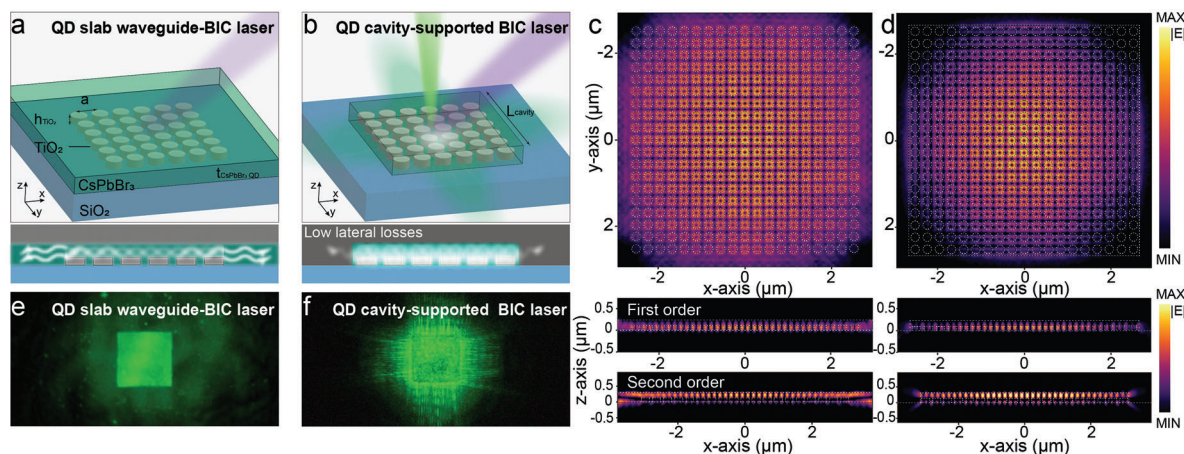


Figure 1. Schematic of a) CsPbBr₃ QD slab waveguide-BIC laser and b) CsPbBr₃ QD cavity-supported BIC laser. Simulated electric field norm distribution of c) QD slab waveguide-BIC laser and d) QD cavity-supported BIC laser with 19×19 unit cells. The top figures are first-order modes in the x-y plane. Middle figures are first-order modes in the x-z plane. The bottom figures are second-order modes in the x-z plane. e) and f) Micro-PL image of a CsPbBr₃ QD slab waveguide-BIC laser and a CsPbBr₃ QD cavity-supported BIC laser. The CsPbBr₃ QD cavity-supported BIC laser shows a strong lasing emission under a lower pump energy density.

BIC lasers have been realized from some non-solution-processed gain media, such as by fabricating a suspended cavity with a minimum cavity size of $\approx 10 \mu\text{m}$,^[40] introducing a surrounded photonic crystal as a bandgap to decrease the lateral optical losses and shrink the cavity size to $\approx 2.5 \mu\text{m}$,^[41,42] and designing Fano-BIC cavity based on photonic crystals with a cavity size down to $\approx 2 \mu\text{m}$.^[43] These miniaturized BIC lasers showed impressive results while the use of the surrounded boundary photonic crystal requires a larger device size and careful design of the photonic crystal. For conventional solution-processed BIC lasers, except for some BIC lasers based on direct pattern metasurface,^[5] the gain medium is usually spin-coated on top of the nanostructure to form a thin film and acts as a slab waveguide.^[1,2,12,44,45] The BIC modes arise from slab waveguide modes in the thin film and are coupled to the periodic nanocylinder array, which is referred to as slab waveguide BIC laser.^[12] In this case, the leakage of light through the sides becomes more pronounced, especially as the entire cavity's size decreases, thus presenting a challenge for achieving miniaturized BIC lasers based on solution-processed gain media.

Here, we integrate an isolated CsPbBr₃ QD cavity instead of a QD film on top of the TiO₂ nanocylinder array to achieve a QD cavity-supported BIC laser. Different from those miniaturized BIC lasers that utilize surrounded boundary photonic crystals, the direct fabrication of well-defined QD patterns of QDs via a solution process allows us to take advantage of the pattern edges to reduce losses through the cavity edges without the need for carefully designed photonic crystals. We report a single-mode BIC laser by using CsPbBr₃ QDs with a narrow linewidth of around 0.1 nm . Compared with the conventional QD slab-based BIC laser, the proposed QD slab waveguide-BIC laser consisting of the CsPbBr₃ QD cavity-supported BIC laser maintained a low lasing threshold for small cavity sizes. Importantly, a miniaturized BIC laser with a device size down to $10 \times 10 \mu\text{m}^2$ is achieved using the proposed CsPbBr₃ QD cavity-supported BIC laser design, which is the smallest among the existing solution-processed BIC laser. This work provides a strategy

to develop ultra-compact BIC laser via solution-processed gain media.

2. Results and Discussion

Figures 1a and b give the schematic of the conventional CsPbBr₃ QD slab waveguide-BIC laser and CsPbBr₃ QD cavity-supported BIC laser. For the QD slab waveguide-BIC laser, a large area of QD film is coated on the TiO₂ nanocylinder array. Unlike the CsPbBr₃ QD slab waveguide-BIC laser, the CsPbBr₃ QD cavity-supported BIC laser possesses boundaries along its four sides (see Figure S1, Supporting Information for the fabrication process). Figures 1c and d give the simulated near field distribution of first- and second-order BIC modes of a cavity with 19×19 unit cells in the x-y plane (top) and x-z plane (bottom). The second-order BIC mode in the x-y plane is shown in Figure S2 (Supporting Information). The simulation results show that the QD slab waveguide-BIC laser shows higher optical losses in the lateral direction because the QD layer can serve as a waveguide and guide the light away from the cavity. The optical losses are more pronounced in the second-order BIC mode as higher-order BIC modes typically propagate within the slab waveguide and are more susceptible to size constraints and edge effects than first-order BIC modes. Due to the existence of side edges in the CsPbBr₃ QD cavity-supported BIC laser, the lasing mode is better confined within the cavity and shows lower scattering losses in the far field. It is worth noting that different from the conventional microdisk laser with in-plane WGM mode or the reported nanowire F-P laser with direction emission diffracted by top nanograting,^[46,47] the optical feedback still mainly comes from the nanocylinder array. Figures S3a and b (Supporting Information) present the top-view and 30° tilted SEM images of the fabricated TiO₂ nanocylinder array, respectively, where the geometry and the height of the nanocylinder array can be observed. Figures S3c and d (Supporting Information) show the SEM images CsPbBr₃ QD cavity fabricated on the TiO₂ nanocylinder array. From the enlarged SEM image shown in Figure S3d

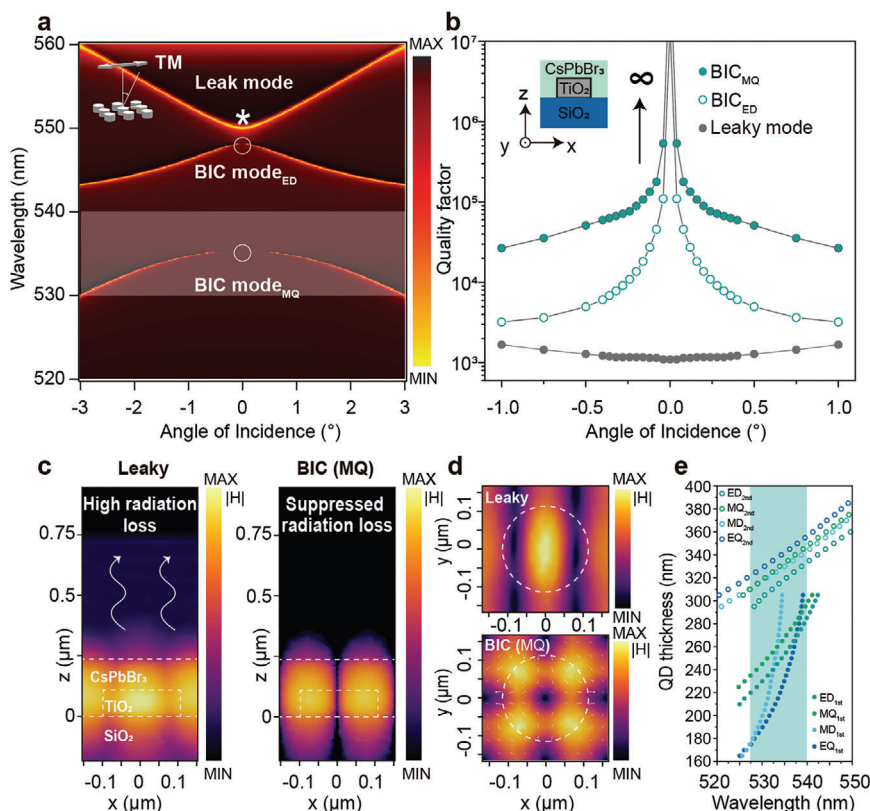


Figure 2. a) Simulated transmission band diagram of first-order mode for the CsPbBr₃ QD-TiO₂ nanocylinder array under TM polarized incident light. The emission band of CsPbBr₃ QD film is indicated by a semi-transparent white color. Lattice parameter, $a = 305$ nm, $d_{\text{TiO}_2} = 220$ nm, $h_{\text{TiO}_2} = 120$ nm, $t_{\text{QD}} = 240$ nm. b) Simulated Q factor as a function of the incident angle of the first-order BIC mode, derived from Figure a. c) Simulated magnetic field norm distributions in the x-z plane of the leaky mode and the MQ BIC mode. The scale bar is in the log scale. d) Simulated magnetic field norm distributions in the x-y plane of the leaky mode and the MQ BIC mode. e) Simulated BIC mode resonance wavelength of the CsPbBr₃ QD-TiO₂ nanocylinder array as a function of the QD film thickness.

(Supporting Information), the CsPbBr₃ QD cavity is well aligned on the TiO₂ nanocylinder array. Finally, micro-PL images of the CsPbBr₃ QD slab waveguide-BIC laser and CsPbBr₃ QD cavity-supported BIC laser with a cavity size of $20 \times 20 \mu\text{m}^2$ are shown in Figures 1e and f. Note that the pump energy density is around $40 \mu\text{J cm}^{-2}$. Due to the lateral loss in the QD layer, only lasing from the CsPbBr₃ QD cavity-supported BIC laser is observed here.

Figure 2a shows the simulated transmission band diagram of the CsPbBr₃ QD coated TiO₂ nanocylinder array under TM-polarized incident light with a cylinder diameter $d_{\text{TiO}_2} = 220$ nm, cylinder height $h_{\text{TiO}_2} = 120$ nm, period $a = 305$ nm, and QD thickness $t_{\text{QD}} = 240$ nm. The emission band of CsPbBr₃ QDs is indicated with a semi-transparent white color in the figure. Under this condition, the first-order BIC mode is excited within the emission band of CsPbBr₃ QD. Note that by engineering the lattice parameters and QD thickness, the second-order BIC modes can also be shifted to match the emission band of the QD, as shown in the Supporting Information. The mode at normal incidence on the upper band is referred to as the diffraction-coupled band-edge mode, referred to as the leaky mode in the following, in which light can couple with the outgoing field and radiate. The dark modes at the middle and bottom band are referred to as electric dipole (ED) BIC mode and magnetic quadrupole (MQ) BIC

mode. The theoretical Q factors of the leaky mode and BIC modes presented in Figure 2b are derived from the simulated dispersion band diagram of Figure 2a. Compared with the leaky mode which possesses a low Q factor, the BIC modes show extremely high Q factors which increase toward infinity as the angle of incidence approaches zero. The simulated near-field distributions of the leaky and MQ BIC modes in the x-z plane and x-y plane are shown in Figures 2c and d, respectively. The mode distributions of ED, magnetic dipole (MD), and electric quadrupole (EQ) BIC modes are also demonstrated in Figure S6 of the Supporting Information. The leaky mode shows strong far-field radiation losses, while the far-field radiation losses in the BIC mode are highly suppressed, which also explains the extremely high Q factor of this BIC mode. This simulation assumes no absorption in all materials of the investigated system, no scattering losses, and an infinitely extended lattice period. However, in the real case, the absorption of material, fabrication defects, and the finite size of the cavity need to be considered. Consequently, the Q factor for the quasi-BIC mode becomes finite. Figure 2e shows the simulated BIC mode resonance wavelengths of the first- and second-order of the CsPbBr₃ QD-TiO₂ nanocylinder array as a function of the QD film thickness. For each mode, the lattice parameters are engineered to match the mode with the emission band of CsPbBr₃ QDs (see details in the Supporting Information).

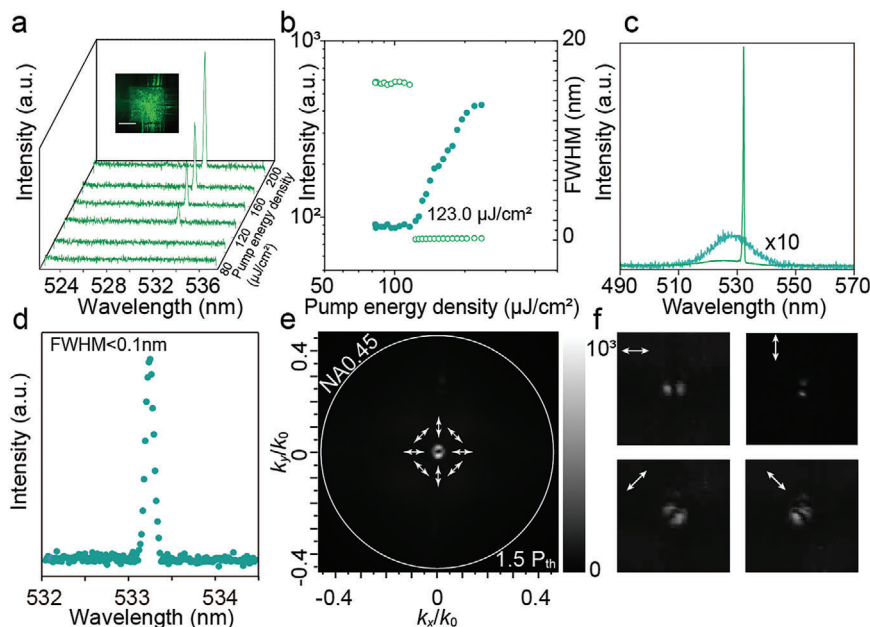


Figure 3. Lasing behavior of the CsPbBr₃ QD cavity-supported BIC laser, as defined in Figure 2. $L_{\text{cavity}} = 40 \mu\text{m}$. a) The emission spectra and b) the emission intensity as a function of the pump energy density. Inset of Figure a is the micro-PL image of the laser above the threshold. The scale bar is $20 \mu\text{m}$. c) Spontaneous emission spectra below lasing threshold ($P < P_{\text{th}}$) and lasing spectra above lasing threshold ($P > 1.8 P_{\text{th}}$) of the CsPbBr₃ QD cavity-supported BIC laser shown over a large wavelength range. d) The high-resolution spectrum of the single-mode lasing ($P > 1.1 P_{\text{th}}$) showing an FWHM of $\approx 0.1 \text{ nm}$. e) The far-field emission pattern collected at the back focal plane of a lens with a numerical aperture (NA) of 0.45. f) Polarization dependence of the far-field radiation pattern for lasing. The direction of polarization of the output beam is marked by the white arrows.

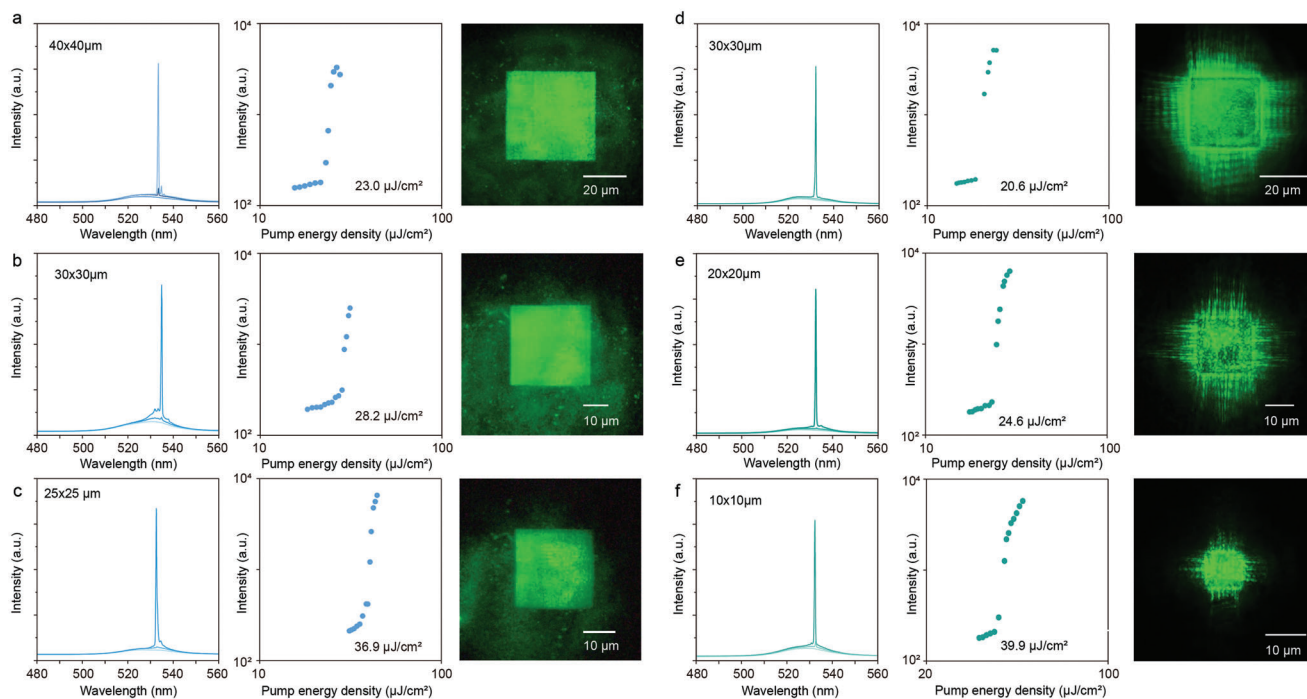


Figure 4. Optical characterizations of the CsPbBr₃ QD slab waveguide-BIC laser and CsPbBr₃ QD cavity-supported BIC laser. a, b, c) Lasing behavior of the CsPbBr₃ QD slab waveguide-BIC laser. d, e, f) Lasing behavior of the CsPbBr₃ QD cavity-supported BIC laser. For each figure, the left figure shows the spontaneous and lasing emission spectra. The middle figure shows the emission intensity as a function of the pump energy density. The right figure shows the micro-PL image of the lasers above the lasing threshold. The parameters of the nanocylinder array and QD thickness have been optimized to match the emission band to the second-order MD BIC mode: cylinder diameter $d_{\text{TiO}_2} = 240 \text{ nm}$, cylinder height $h_{\text{TiO}_2} = 120 \text{ nm}$, period $a = 335 \text{ nm}$, and QD thickness $t_{\text{QD}} = 310 \text{ nm}$.

Table 1. Comparison between BIC lasers.

Gain material	Wavelength [nm]	Q_{lasing}	Pump method	Threshold peak power [mW]	Threshold average power density [kW cm ²]	Smallest cavity size [μm ²]	Smallest device size [μm ²]	Refs.
<i>Non-solution-processed</i>								
InGaAsP MQWs	1551.4	4701	Pulsed pump	15.6	4	9.6 × 9.6	9.6 × 9.6	[40]
InGaAsP MQWs	~1550	—	Pulsed pump	73	—	—	—	[51]
GaAs	825	2750	Pulsed pump	8.8 × 10 ⁵	7.0 × 10 ⁴	—	—	[52]
InGaAsP MQWs	~1620	7300	Pulsed pump	0.34	1.47	23 × 23	23 × 23	[53]
InGaP MQWs	621	2070	Pulsed pump	1.5 × 10 ⁷	7.5 × 10 ⁵	50 × 50	50 × 50	[54]
GaAs MQWs	940	150	Pulsed pump	1.1 × 10 ⁵	—	35 × 10	35 × 10	[55]
GaN	376.5	3765	Pulsed pump	5.2 × 10 ⁵	2.7 × 10 ⁴	8 × 8	8 × 8	[56]
InAs/GaAs epitaxial QDs	1260~1275	32500	cw pump	0.041	0.08	7.5 × 7.5	21 × 21	[42]
InAs/GaAs epitaxial QDs	1303	2327	cw pump	0.012	0.052	2.5 × 2.5	13 × 13	[41]
InGaAsP QWs	1560	78000	cw pump	3.5	12.38	≈2.2	32 × 11	[43]
<i>Solution-processed</i>								
MAPbBr ₃	552	—	Pulsed pump	5.3 × 10 ⁵	4.2 × 10 ⁴	—	—	[5]
CdSe/CdZnS CQDs	647.7	2590	Pulsed pump	5.1 × 10 ⁶	1.8 × 10 ⁵	—	—	[15]
MAPbBr ₃	548.5	1120	Pulsed pump	6.2 × 10 ⁶	4.9 × 10 ⁵	—	—	[6]
Rhodamine 101	614	614	Pulsed pump	7.9 × 10 ³	1.0 × 10 ²	—	—	[48]
CdSe/CdS CQDs	626	—	Pulsed pump	3.1 × 10 ²	11	—	—	[12]
IR-140	878~912	~1820	Pulsed pump	8.3 × 10 ³	20	—	—	[2]
Rhodamine 6G	~600	~1960	Pulsed pump	1.6 × 10 ³	1.0 × 10 ²	—	—	[44]
MAPbI ₃	775	1370	Pulsed pump	—	—	—	—	[4]
MAPbI ₃	791~797	797	Pulsed pump	5.7 × 10 ⁵	8.0 × 10 ⁴	—	—	[7]
MaPbBr ₃	550	1100	Pulsed pump	2.2 × 10 ⁴	1.1 × 10 ³	—	—	[49]
IR-792	~867	1734	Pulsed pump	2.2 × 10 ⁶	2.8 × 10 ⁴	20 × 20	20 × 20	[45]
IR-140	~897	1382	Pulsed pump	1.6 × 10 ⁸	2.2 × 10 ⁶	85 × 85	85 × 85	[50]
CsPbBr ₃ CQDs	532	5320	Pulsed pump	1.6 × 10 ⁴	2.0 × 10 ²	10 × 10	10 × 10	This work

MQWs: multiple quantum wells CQDs: colloidal quantum dots.

First-order BIC modes have a higher tolerance for thickness variation compared with the second-order BIC modes. For the first-order modes, a QD thickness variation of 150 nm can still maintain the BIC mode within the gain emission band. For the second-order modes, the QD thickness variation needs to be controlled within ≈60 nm, which needs more accurate control of the QD thickness in the fabrication process.

The lasing properties of the CsPbBr₃ QD cavity-supported BIC laser (structure parameters indicated in Figure 2) with a finite size of 40 × 40 μm² are characterized at room temperature (see Figure S4, Supporting Information for details about the measurement setup). Figure 3a presents the lasing emission spectrum of the CsPbBr₃ cavity-supported BIC laser under different pump energy densities pumped by a 355-nm nanosecond laser. As the pump energy density increases, the output intensity of the PL band linearly increases. Once the pump energy density reaches the lasing threshold, a single sharp peak appears at 532 nm. Figure 3b gives the emission intensity as a function of the pump energy density. A clear threshold behavior is observed at 123.0 μJ cm⁻². Note that a lasing threshold of 29.6 μJ cm⁻² is observed by pumping the CsPbBr₃ QD cavity-supported BIC

laser using a 400-nm fs laser (Figure S5, Supporting Information). Figure 3c shows the lasing and spontaneous emission spectrum of the CsPbBr₃ QD cavity-supported BIC laser over a large wavelength range. The single-mode lasing peak shows up within the gain region of the CsPbBr₃ QDs. For the CsPbBr₃ QD cavity-supported BIC laser, a best-measured FWHM is ≈0.1 nm. The far-field emission is collected at the back focal plane of a lens with a numerical aperture (NA) of 0.45. The lasing profile from the QD cavity-supported BIC laser shows a dark area in the middle part of the image surrounded by a donut-shape bright ring. The dark area in the middle may be related to suppressed radiation in the strict normal direction for the BIC mode and a topological singularity at the beam axis.^[5,12] The lasing radiated in the vicinity of the BIC mode. The polarization dependence of the far-field lasing profile is also characterized by rotating the linear polarizer in front of the CCD camera as shown in Figure 3f. These results agree well with simulated the electric field direction shown in the near-field distribution in Figure 2d, indicating a lasing is achieved via an MQ BIC mode. The period of the nanocylinder array is engineered to match the ED, MD, and EQ BIC modes to the gain emission band, and lasing emissions for these modes are observed. The far-field emission properties

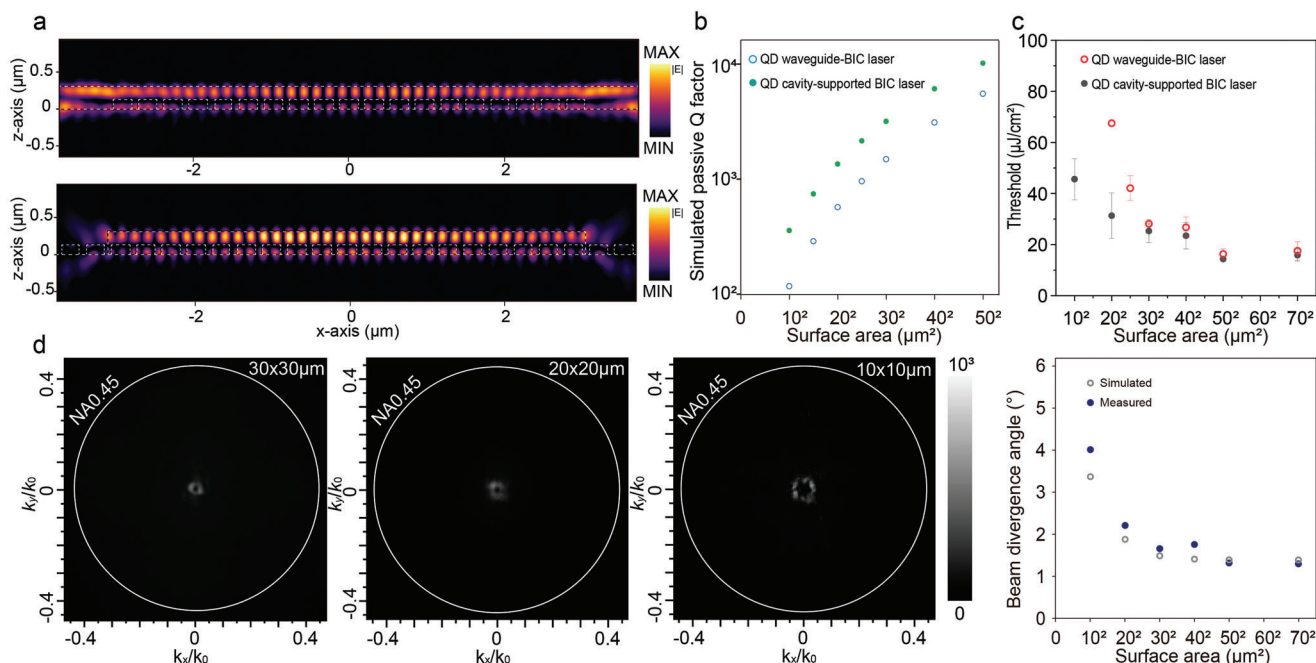


Figure 5. a) Simulated electric field norm distribution of second-order mode for QD slab waveguide-BIC laser (top) and QD cavity-supported BIC laser (bottom) with 19×19 unit cells. The TiO_2 nanocylinders surrounding the QD cavity-supported BIC laser are taken into account here. b) Simulated passive Q factor as a function of the cavity size. c) The lasing threshold of the QD slab waveguide-BIC laser and QD cavity-supported BIC laser for different cavity sizes. d) The experimental far-field emission pattern and corresponding beam divergence angle of CsPbBr_3 QD cavity supported-BIC laser for different cavity sizes.

of the lasing generated from ED, MD, and EQ BIC modes are also characterized in Figure S7 (Supporting Information). The polarization-dependant radiation patterns of these modes match well with the corresponding simulated results. Note that the effect of pump light polarization on lasing emission is not considered in this work.

To investigate the effect of the isolated cavity on the BIC laser, the lasing behavior of the CsPbBr_3 QD slab waveguide-BIC lasers and CsPbBr_3 QD cavity-supported BIC lasers with different cavity sizes are characterized by using a fs laser as a pump (excitation at 400 nm), as shown in Figure 4. Note that here we focus on the second-order MD BIC mode for obvious comparison, as the lateral losses of the high-order mode in infinite-size thin film are higher than that of the first-order mode as mentioned above. The parameters of the nanocylinder array and QD thickness have been optimized to match the emission band to the second-order MD BIC mode: cylinder diameter $d_{\text{TiO}_2} = 240$ nm, cylinder height $h_{\text{TiO}_2} = 120$ nm, period $a = 335$ nm, and QD thickness $t_{\text{QD}} = 310$ nm. The corresponding simulated transmission band diagram and near-field distribution are shown in Figure S8 (Supporting Information). For the CsPbBr_3 QD slab waveguide-BIC lasers, a sharp single-mode lasing within the gain region of CsPbBr_3 QD is observed. The lasing emission intensity as a function of pump energy density also shows a clear threshold behavior. The lasing threshold decreased slightly as the cavity size increased, which could be attributed to better confinement from the lattice and a higher gain contribution from the QD. Note that the minimum size that exhibits a lasing is $20 \mu\text{m}$ for CsPbBr_3 QD slab waveguide-BIC lasers as shown in Figure S9 (Supporting Information). When increasing the pump energy density, a broad

peak initially appears on the PL. Once the pump energy density reaches $67.5 \mu\text{J cm}^{-2}$, a relatively sharp peak which should likely correspond to the lasing onset of the BIC-supported mode is observed. For the CsPbBr_3 QD cavity-supported BIC lasers, besides the single-mode lasing, a lower threshold behavior is observed compared with the same-size CsPbBr_3 QD slab waveguide-BIC lasers. This may be due to the better lateral confinement from the isolated cavity. The optical microscope images showing the lasers above their lasing thresholds are given in the right part of each figure. The CsPbBr_3 QD cavity-supported BIC laser exhibits a low lateral loss, however, from the optical image, scattering light is only observed from the edge of the CsPbBr_3 QD cavity-supported BIC laser. For the CsPbBr_3 QD slab waveguide-BIC laser, the QD layer can act as a waveguide and guide light in the lateral direction so that less scattered light can be observed from the objective lens. Note that the minimum device size that exhibits lasing is $10 \times 10 \mu\text{m}^2$ for CsPbBr_3 QD cavity-supported BIC lasers, which is the smallest BIC laser among the BIC lasers based on solution-processed gain media and also comparable with the non-solution-processed BIC lasers (Table 1).^[2,4-7,12,15,40-45,48-56]

To further investigate the isolated cavity effect, simulated near-field distributions for the CsPbBr_3 QD slab waveguide-BIC laser and CsPbBr_3 QD cavity-supported BIC laser are presented in Figure 5a. In this case, TiO_2 nanocylinders surrounding the QD cavity are taken into account to match the real case. We also performed simulations to investigate the effect of different edge conditions and surface roughness on the passive Q factor of the CsPbBr_3 QD cavity-supported BIC laser as shown in Figures S10 and Figure S12 (Supporting Information). For the CsPbBr_3 QD slab waveguide-BIC laser, light being guided out of the

nanostructure is observed and thus larger optical losses are to be expected. This can also be confirmed by the observation of scattered light under lasing operation, as shown in Figure S11 (Supporting Information). For the CsPbBr₃ QD cavity-supported BIC laser, light is better confined within the slab and only a little light is found to be scattered at the edge. The simulated Q factor of the CsPbBr₃ QD slab waveguide-BIC laser and CsPbBr₃ QD cavity-supported BIC laser with different cavity sizes are presented in Figure 5b. The CsPbBr₃ QD cavity-supported BIC laser shows a higher Q factor compared with that of the CsPbBr₃ QD slab waveguide-BIC laser, especially for smaller cavity sizes (≈ 3 times for a size of $10 \times 10 \mu\text{m}^2$). Figure 5c gives the measured lasing threshold power of the lasers under different cavity sizes. The threshold difference becomes large when the cavity size is below $20 \mu\text{m}$. As the cavity size increases, the difference in threshold becomes small, which can be explained by the improvement in the confinement with the number of unit cells, and the effect of lateral confinement with and without boundary becomes negligible. The far-field emission patterns of the corresponding CsPbBr₃ QD cavity-supported BIC laser are shown in Figure 5d. The beam divergence of the lasing beam becomes larger as the cavity size decreases, which agrees well with the simulation results.

3. Conclusion

In conclusion, we demonstrate a CsPbBr₃ QD cavity-supported BIC laser by integrating an isolated CsPbBr₃ QD cavity on a TiO₂ nanocylinder array. A small footprint single mode BIC laser with a narrow linewidth of $\approx 0.1 \text{ nm}$ is realized. By engineering the lattice parameters, BIC lasing generated from ED, MD, EQ, and MQ modes are observed. Compared with the conventional CsPbBr₃ QD slab waveguide-BIC laser, the CsPbBr₃ QD cavity-supported BIC laser shows a lower lasing threshold, especially at a small footprint size. Finally, lasing with a miniaturized BIC laser having a device size down to $10 \times 10 \mu\text{m}^2$ is achieved owing to the decreased lateral optical losses.

Supporting Information

Supporting Information is available from the Wiley Online Library or from the author.

Acknowledgements

This work was supported by JSPS KAKENHI (JP21H01383, JP23KF0107, JP23H01461). "Advanced Research Infrastructure for Materials and Nanotechnology in Japan (ARIM)" of the Ministry of Education, Culture, Sports, Science and Technology (MEXT) (Proposal Number JP-MXP1223UT1077). The authors would like to extend their grateful appreciation to Prof. Kuniaki Konishi and Prof. Junji Yumoto from the School of Science, The University of Tokyo for technical support.

Conflict of Interest

The authors declare no conflict of interest.

Data Availability Statement

The data that support the findings of this study are available from the corresponding author upon reasonable request.

Keywords

bound states in the continuum, CsPbBr₃ quantum dots, low lateral-loss cavity, miniaturized lasers, solution-processed lasers

Received: November 25, 2023

Revised: January 22, 2024

Published online:

- [1] S. I. Azzam, K. Chaudhuri, A. Lagutchev, Z. Jacob, Y. L. Kim, V. M. Shalae, A. Boltasseva, A. V. Kildishev, *Laser Photonics Rev.* **2021**, *15*, 2000411.
- [2] Z. Zhai, Z. Li, Y. Du, X. Gan, L. He, X. Zhang, Y. Zhou, J. Guan, Y. Cai, X. Ao, *ACS Photonics* **2023**, *10*, 437.
- [3] J.-H. Yang, Z.-T. Huang, D. N. Maksimov, P. S. Pankin, I. V. Timofeev, K.-B. Hong, H. Li, J.-W. Chen, C.-Y. Hsu, Y.-Y. Liu, T.-C. Lu, T.-R. Lin, C.-S. Yang, K.-P. Chen, *Laser Photonics Rev.* **2021**, *15*, 2100118.
- [4] C.-C. Liu, H.-H. Hsiao, Y.-C. Chang, *Sci. Adv.* **2023**, *9*, eadf6649.
- [5] C. Z. Can Huang, S. Xiao, Y. Wang, Y. Fan, Y. Liu, N. Zhang, G. Qu, H. Ji, J. Han, L. Ge, Y. Kivshar, Q. Song, *Science* **2020**, *367*, 1018.
- [6] Y. Wang, Y. Fan, X. Zhang, H. Tang, Q. Song, J. Han, S. Xiao, *ACS Nano* **2021**, *15*, 7386.
- [7] J. Tian, G. Adamo, H. Liu, M. Wu, M. Klein, J. Deng, N. S. S. Ang, R. Paniagua-Domínguez, H. Liu, A. I. Kuznetsov, C. Soci, *Adv. Mater.* **2023**, *35*, 2207430.
- [8] C. Qin, A. S. D. Sandanayaka, C. Zhao, T. Matsushima, D. Zhang, T. Fujihara, C. Adachi, *Nature* **2020**, *585*, 53.
- [9] J. Yu, M. Sharma, M. Li, S. Delikanli, A. Sharma, M. Taimoor, Y. Altintas, J. R. McBride, T. Kusserow, T.-C. Sum, H. V. Demir, C. Dang, *Laser Photonics Rev.* **2021**, *15*, 2100034.
- [10] R. Duan, Z. Zhang, L. Xiao, X. Zhao, Y. T. Thung, L. Ding, Z. Liu, J. Yang, V. D. Ta, H. Sun, *Adv. Mater.* **2022**, *34*, 2108884.
- [11] Z. Yang, M. Pelton, I. Fedin, D. V. Talapin, E. Waks, *Nat. Commun.* **2017**, *8*, 143.
- [12] M. Wu, L. Ding, R. P. Sabatini, L. K. Sagar, G. Bappi, R. Paniagua-Dominguez, E. H. Sargent, A. I. Kuznetsov, *Nano Lett.* **2021**, *21*, 9754.
- [13] H. Chang, Y. Zhong, H. Dong, Z. Wang, W. Xie, A. Pan, L. Zhang, *Light Sci. Appl.* **2021**, *10*, 60.
- [14] M. M. Adachi, F. Fan, D. P. Sellan, S. Hoogland, O. Voznyy, A. J. Houtepen, K. D. Parrish, P. Kanjanaboos, J. A. Malen, E. H. Sargent, *Nat. Commun.* **2015**, *6*, 8694.
- [15] M. Wu, S. T. Ha, S. Shendre, E. G. Durmusoglu, W. K. Koh, D. R. Abujetas, J. A. Sanchez-Gil, R. Paniagua-Dominguez, H. V. Demir, A. I. Kuznetsov, *Nano Lett.* **2020**, *20*, 6005.
- [16] J. Guan, L. K. Sagar, R. Li, D. Wang, G. Bappi, W. Wang, N. Watkins, M. R. Bourgeois, L. Levina, F. Fan, S. Hoogland, O. Voznyy, J. M. de Pina, R. D. Schaller, G. C. Schatz, E. H. Sargent, T. W. Odom, *ACS Nano* **2020**, *14*, 3426.
- [17] J. Roh, Y.-S. Park, J. Lim, V. I. Klimov, *Nat. Commun.* **2020**, *11*, 271.
- [18] G. L. Whitworth, M. Dalmas, N. Taghipour, G. Konstantatos, *Nat. Photonics* **2021**, *15*, 738.
- [19] W. Xie, T. Stöferle, G. Rainò, T. Aubert, S. Bisschop, Y. Zhu, R. F. Mahrt, P. Geiregat, E. Brainis, Z. Hens, D. Van Thourhout, *Adv. Mater.* **2017**, *29*, 1604866.
- [20] P. J. Cegielski, A. L. Giesecke, S. Neutzner, C. Porschatis, M. Gandini, D. Schall, C. A. R. Perini, J. Bolten, S. Suckow, S. Kataria, B. Chmielak, T. Wahlbrink, A. Petrozza, M. C. Lemme, *Nano Lett.* **2018**, *18*, 6915.
- [21] J. Guan, R. Li, X. G. Juarez, A. D. Sample, Y. Wang, G. C. Schatz, T. W. Odom, *Adv. Mater.* **2023**, *35*, 2103262.
- [22] S. Chen, K. Roh, J. Lee, W. K. Chong, Y. Lu, N. Mathews, T. C. Sum, A. Nurmikko, *ACS Nano* **2016**, *10*, 3959.

- [23] J. Zhao, Y. Yan, Z. Gao, Y. Du, H. Dong, J. Yao, Y. S. Zhao, *Nat. Commun.* **2019**, *10*, 870.
- [24] Y. Wang, S. Chen, Y. Yu, L. Zhou, L. Liu, C. Yang, M. Liao, M. Tang, Z. Liu, J. Wu, W. Li, I. Ross, A. J. Seeds, H. Liu, S. Yu, *Optica* **2018**, *5*, 528.
- [25] A. Rose, Z. Zhu, C. F. Madigan, T. M. Swager, V. Bulović, *Nature* **2005**, *434*, 876.
- [26] F. Vollmer, S. Arnold, *Nat. Methods* **2008**, *5*, 591.
- [27] Z. Hu, Z. Liu, Z. Zhan, T. Shi, J. Du, X. Tang, Y. Leng, *Adv. Photonics* **2021**, *3*, 034002.
- [28] B. R. Sutherland, E. H. Sargent, *Nat. Photonics* **2016**, *10*, 295.
- [29] Q. A. Akkerman, G. Raino, M. V. Kovalenko, L. Manna, *Nat. Mater.* **2018**, *17*, 394.
- [30] S. Yakunin, L. Protesescu, F. Krieg, M. I. Bodnarchuk, G. Nedelcu, M. Humer, G. De Luca, M. Fiebig, W. Heiss, M. V. Kovalenko, *Nat. Commun.* **2015**, *6*, 8056.
- [31] H. Huang, L. Polavarapu, J. A.ichert, A. S. Susha, A. S. Urban, A. L. Rogach, *NPG Asia Mater* **2016**, *8*, e328.
- [32] Y. Xu, Q. Chen, C. Zhang, R. Wang, H. Wu, X. Zhang, G. Xing, W. W. Yu, X. Wang, Y. Zhang, M. Xiao, *J. Am. Chem. Soc.* **2016**, *138*, 3761.
- [33] Y. H. Hsieh, B. W. Hsu, K. N. Peng, K. W. Lee, C. W. Chu, S. W. Chang, H. W. Lin, T. J. Yen, Y. J. Lu, *ACS Nano* **2020**, *14*, 11670.
- [34] C.-Y. Huang, C. Zou, C. Mao, K. L. Corp, Y.-C. Yao, Y.-J. Lee, C. W. Schlenker, A. K. Y. Jen, L. Y. Lin, *ACS Photonics* **2017**, *4*, 2281.
- [35] M. J. H. Tan, Y. Wang, Y. Chan, *Appl. Phys. Lett.* **2019**, *114*, 183101.
- [36] C. W. Hsu, B. Zhen, A. D. Stone, J. D. Joannopoulos, M. Soljačić, *Nat. Rev. Mater.* **2016**, *1*, 16048.
- [37] C. W. Hsu, B. Zhen, J. Lee, S. L. Chua, S. G. Johnson, J. D. Joannopoulos, M. Soljacic, *Nature* **2013**, *499*, 188.
- [38] Y. Plotnik, O. Peleg, F. Dreisow, M. Heinrich, S. Nolte, A. Szameit, M. Segev, *Phys. Rev. Lett.* **2011**, *107*, 183901.
- [39] A. Taghizadeh, I.-S. Chung, *Appl. Phys. Lett.* **2017**, *111*, 031114.
- [40] A. Kodigala, T. Lepetit, Q. Gu, B. Bahari, Y. Fainman, B. Kante, *Nature* **2017**, *541*, 196.
- [41] H. Zhong, Y. Yu, Z. Zheng, Z. Ding, X. Zhao, J. Yang, Y. Wei, Y. Chen, S. Yu, *Light Sci. Appl.* **2023**, *12*, 100.
- [42] Y. Ren, P. Li, Z. Liu, Z. Chen, Y.-L. Chen, C. Peng, J. Liu, *Sci. Adv.* **2022**, *8*, eade8817.
- [43] Y. Yu, A. Sakanas, A. R. Zali, E. Semenova, K. Yvind, J. Mørk, *Nat. Photonics* **2021**, *15*, 758.
- [44] J. H. Yang, Z. T. Huang, D. N. Maksimov, P. S. Pankin, I. V. Timofeev, K. B. Hong, H. Li, J. W. Chen, C. Y. Hsu, Y. Y. Liu, T. C. Lu, T. R. Lin, C. S. Yang, K. P. Chen, *Laser Photonics Rev.* **2021**, *15*, 2100118.
- [45] S. Mohamed, J. Wang, H. Rekola, J. Heikkinen, B. Asamoah, L. Shi, T. K. Hakala, *Laser Photonics Rev.* **2022**, *16*, 2100574.
- [46] A. Zhizhchenko, S. Syubaev, A. Berestennikov, A. V. Yulin, A. Porfirev, A. Pushkarev, I. Shishkin, K. Golokhvast, A. A. Bogdanov, A. A. Zakhidov, A. A. Kuchmizhak, Y. S. Kivshar, S. V. Makarov, *ACS Nano* **2019**, *13*, 4140.
- [47] A. Y. Zhizhchenko, A. B. Cherepakhin, M. A. Masharin, A. P. Pushkarev, S. A. Kulinich, A. A. Kuchmizhak, S. V. Makarov, *Nano Lett.* **2021**, *21*, 10019.
- [48] S. I. Azzam, K. Chaudhuri, A. Lagutchev, Z. Jacob, Y. L. Kim, V. M. Shalae, A. Boltasseva, A. V. Kildishev, *Laser Photonics Rev.* **2021**, *15*, 2000411.
- [49] R. Mermet-Lyauoz, C. Symonds, F. Berry, E. Drouard, C. Chevalier, G. Trippé-Allard, E. Deleporte, J. Bellessa, C. Seassal, H. S. Nguyen, *Nano Lett.* **2023**, *23*, 4152.
- [50] R. Heilmann, G. Salerno, J. Cuerda, T. K. Hakala, P. Torma, *ACS Photonics* **2022**, *9*, 224.
- [51] F. V. B. Bahari, T. Lepetit, R. Tellez-Limon, J. H. Park, A. Kodigala, Y. Fainman, B. Kante, arXiv: optics, **2017**, <https://arxiv.org/abs/1707.00181>.
- [52] S. T. Ha, Y. H. Fu, N. K. Emani, Z. Pan, R. M. Bakker, R. Paniagua-Dominguez, A. I. Kuznetsov, *Nat. Nanotechnol.* **2018**, *13*, 1042.
- [53] M. S. Hwang, H. C. Lee, K. H. Kim, K. Y. Jeong, S. H. Kwon, K. Koshelev, Y. Kivshar, H. G. Park, *Nat. Commun.* **2021**, *12*, 4135.
- [54] S. T. Ha, R. Paniagua-Dominguez, A. I. Kuznetsov, *Adv. Opt. Mater.* **2022**, *10*, 2200753.
- [55] H. Zhen-Ting, C. Chiao-Yun, C. Kuo-Ping, L. Tien-Chang, *Adv. Photonics* **2022**, *4*, 066004.
- [56] M.-H. Chen, D. Xing, V.-C. Su, Y.-C. Lee, Y.-L. Ho, J.-J. Delaunay, *Adv. Opt. Mater.* **2023**, *11*, 2201906.